TECHNICAL RESEARCH REPORT

Sampled-Data Modeling and Analysis of PWM DC-DC Converters Part II. The Power Stage

by C.-C. Fang, E.H. Abed

T.R. 98-55

Sampled-Data Modeling and Analysis of PWM DC-DC Converters II. The Power Stage

Chung-Chieh Fang and Eyad H. Abed
Department of Electrical Engineering
and the Institute for Systems Research
University of Maryland
College Park, MD 20742 USA

Abstract

The power stage of the PWM DC-DC converter is modeled and analyzed using the sampled-data approach. This work complements the companion paper [1] which develops sampled-data models and analysis for the closed-loop converter. Separate models for the power stage are essential for controller design. The work addresses continuous and discontinuous conduction mode under voltage mode control, and continuous conduction mode under current mode control. For each configuration, nonlinear and linearized sampled-data models, and control-to-output transfer function are derived. Use of these models for controller design is illustrated. In addition, a new continuous-time switching frequency-dependent model of the power stage is derived from the sampled-data model. Examples illustrate the increased accuracy of control design using the new power stage models.

1 Introduction

A DC-DC converter consists of a power stage and a controller, as shown in Fig. 1. To design the controller, it is essential to have a good model of the power stage. In this paper, Sampled-data modeling and analysis of the power stage of the PWM DC-DC converter is pursued. A similar study was performed in the companion paper [1] for closed-loop PWM DC-DC converters. Closed-loop modeling and analysis are useful for performance evaluation. On the other hand, open-loop modeling and analysis are critical for control design.

The organization of the paper is as follows. In Sec. 2, the power stage in continuous conduction mode (CCM) under voltage mode control is studied. The steps of sampled-data approach in [1] are followed in details. In Sec. 3 and 4, the power stages in discontinuous conduction mode (DCM) under voltage mode control, and CCM under current mode control, respectively, are studied. In Sec. 5, a new approach to derive linear continuous-time models of PWM converter power stage

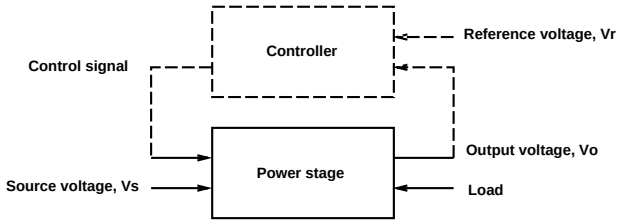

Figure 1: System diagram of a DC-DC converter

from sampled-data models is proposed. In Sec. 6, numerous illustrative examples are given. Better prediction of closed-loop performance by using sampled-data model of the power stage is shown.

2 Continuous Conduction Mode (CCM) under Voltage Mode Control

2.1 Block Diagram Model

A block diagram model of the power stage of a PWM converter operated in CCM under voltage mode control is shown in Fig. 2, where $d_n \in \mathbf{R}$ is the switching instant within the cycle and is used as the control variable, $A_1, A_2 \in \mathbf{R}^{N\times N}$, $B_1, B_2 \in \mathbf{R}^{N\times 1}$, $E_1, E_2 \in \mathbf{R}^{1\times N}$, are constant matrices, T is the constant switching period (inverse of switching frequency f_s), and v_s, $v_o \in \mathbf{R}$ are the source and output voltages, respectively.

2.2 Nonlinear Sampled-Data Model

Generally in the PWM converter, the switching frequency is sufficiently high that the variations in v_s in a cycle can be neglected. Consider the cycle $t \in [nT, (n+1)T)$, take v_s to be constant within the cycle and denote it as v_{sn}. Let $x_n = x(nT)$ and $v_{on} = v_o(nT)$. From the operation in Fig. 2, the sampled-data dynamics of the power stage is

$$\begin{aligned} x_{n+1} &= f(x_n, v_{sn}, d_n) \\ &= e^{A_2(T-d_n)}(e^{A_1 d_n}x_n + \int_0^{d_n} e^{A_1\sigma}d\sigma B_1 v_{sn}) + \int_0^{T-d_n} e^{A_2\sigma}d\sigma B_2 v_{sn} \end{aligned} \tag{1}$$

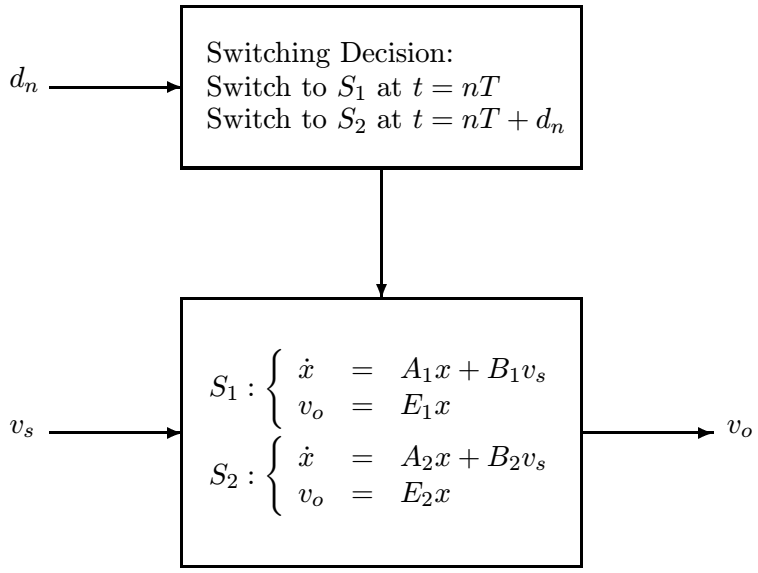

Figure 2: Power stage of PWM converter in CCM under voltage mode control

$$v_{on} = Ex_n \tag{2}$$

where $E = E_1$, E_2, or $(E_1 + E_2)/2$ depending on which output voltage is of interest.

2.3 Existence and Analysis of Periodic Solutions

A T-periodic solution $x^0(t)$ for the system in Fig. 2 corresponds to a fixed point of the sampled-data model. The fixed point $(x_n, v_{sn}, d_n) = (x^0(0), V_s, d)$, if it exists, must satisfy

$$\begin{aligned} x^0(0) &= f(x^0(0), V_s, d) \\ &= e^{A_2(T-d)}(e^{A_1 d}x^0(0) + \int_0^d e^{A_1\sigma}d\sigma B_1 V_s) + \int_0^{T-d} e^{A_2\sigma}d\sigma B_2 V_s \end{aligned} \tag{3}$$

Let the nominal (set-point) output voltage be $V_{\rm SET}$. Assume there is little variation in $x^0(t)$ for $t \in [0, T]$. Then

$$Ex^0(0) = V_{\rm SET} \tag{4}$$

The $N+1$ equations ((3) and (4)) in in $N+1$ unknowns ($x^0(0)$ and d) can be solved by Newton's method [2].

Next the existence of fixed points in the sampled-data dynamics is studied. Assuming all of the eigenvalues of A_1 and A_2 are in the open left half of the complex plane, it follows that the matrices $I - e^{A_2(T-d)}e^{A_1 d}$ and $I - e^{A_1 d}e^{A_2(T-d)}$ are invertible [3]. From Eq. (3), $x^0(0)$ can be expressed as a function $X(d)$ of d:

$$X(d) := (I - e^{A_2(T-d)}e^{A_1 d})^{-1}(e^{A_2(T-d)}\int_0^d e^{A_1\sigma}d\sigma B_1 V_s + \int_0^{T-d} e^{A_2\sigma}d\sigma B_2 V_s) \tag{5}$$

So the $n+1$ equations, (3) and (4), reduce to one equation in one unknown d:

$$EX(d) = V_{\rm SET} \tag{6}$$

Next, a sufficient condition is given for the existence of a periodic solution achieving the nominal output voltage $V_{\rm SET}$.

Theorem 1 *Assume that all of the eigenvalues of A_1 and A_2 are in the open left half of the complex plane. Given the nominal output voltage $V_{\rm SET}$, suppose*

$$(EA_2^{-1}B_2V_s + V_{\rm SET})(EA_1^{-1}B_1V_s + V_{\rm SET}) < 0 \tag{7}$$

Then there exists a periodic solution $x^0(t)$ in the power stage of Fig. 2 with $Ex^0(0) = V_{\rm SET}$.

Proof:

$$X(0) = -A_2^{-1}B_2V_s \tag{8}$$

$$X(T) = -A_1^{-1}B_1V_s \tag{9}$$

From Eq. (6), if

$$\begin{aligned}&(EX(0) - V_{\rm SET})(EX(T) - V_{\rm SET})\\ &= (EA_2^{-1}B_2V_s + V_{\rm SET})(EA_1^{-1}B_1V_s + V_{\rm SET})\\ &< 0\end{aligned}$$

then by the Intermediate Value Theorem, there exists a solution d satisfying Eq. (6). Hence there exists a periodic solution $x^0(t)$. □

2.4 Linearized Sampled-Data Dynamics

When there exists a periodic solution $x^0(t)$, or equivalently a fixed point $(x^0(0), V_s, d)$, the system can be linearized at this fixed point (similar analysis has been done in [4] for the case in which A_1 and A_2 are invertible):

$$\hat{x}_{n+1} \approx \Phi_o \hat{x}_n + \Gamma_v \hat{v}_{sn} + \Gamma_d \hat{d}_n \tag{10}$$

$$\hat{v}_{on} = E\hat{x}_n \tag{11}$$

where

$$\Phi_o = \left.\frac{\partial f}{\partial x_n}\right|_\diamond = e^{A_2(T-d)}e^{A_1 d} \tag{12}$$

$$\Gamma_v = \left.\frac{\partial f}{\partial v_{sn}}\right|_\diamond = e^{A_2(T-d)}\int_0^d e^{A_1\sigma}d\sigma B_1 + \int_0^{T-d} e^{A_2\sigma}d\sigma B_2 \tag{13}$$

$$\begin{aligned}\Gamma_d = \left.\frac{\partial f}{\partial d_n}\right|_\diamond &= e^{A_2(T-d)}((A_1 - A_2)x^0(d) + (B_1 - B_2)V_s) \\ &= e^{A_2(T-d)}(\dot{x}^0(d^-) - \dot{x}^0(d^+))\end{aligned} \tag{14}$$

(the notation $\diamond$ denotes evaluation at $(x_n, v_{sn}, d_n) = (x^0(0), V_s, d)$)

This linearized model is useful for discrete-time feedback control designs. Many different discrete-time control schemes for PWM converters have been proposed and illustrated in [3, 5].

2.5 Control-to-Output Transfer Function

Analog feedback control designs are generally based on the control-to-output transfer function (frequency response).

Previous works using the sampled-data modeling [6, for example] generally use the following as the control-to-output transfer function (derived from Eqs. (10) and (11))

$$\frac{\hat{v}_o(z)}{\hat{d}(z)} = E(zI - \Phi_o)^{-1}\Gamma_d \tag{15}$$

In this approach, the control (switching) exerted at $t = nT + d_n$ occurs *after* the sampling of the output at $t = nT$. This renders the model noncausal. This error in the time domain will cause an error in the phase response.

To circumvent this problem, the output $v_o(nT + d_n)$ (instead of $v_o(nT)$) is used, because the output around $t = nT + d_n$ determines the switching action. The output equation (2) now becomes

$$v_{on} = Ex(nT + d_n) = E(e^{A_1 d_n} x_n + \int_0^{d_n} e^{A_1 \sigma} d\sigma B_1 v_{sn}) \tag{16}$$

with linearized dynamics

$$\hat{v}_{on} \approx E(e^{A_1 d} \hat{x}_n + \dot{x}^0(d^-)\hat{d}_n + \int_0^{d} e^{A_1 \sigma} d\sigma B_1 \hat{v}_{sn}) \tag{17}$$

From the linearized dynamics (10) and (17), the control-to-output transfer function is

$$T_{oc}(z) = \frac{\hat{v}_o(z)}{\hat{d}(z)} = Ee^{A_1 d}(zI - \Phi_o)^{-1}\Gamma_d + E\dot{x}^0(d^-) \tag{18}$$

Given a transfer function in z domain, say $T(z)$, its effective frequency response [7, p. 93] is $T(e^{j\omega T})$, which is valid in the frequency range $|\omega| < \frac{\pi}{T}$. In the case when v_o is discontinuous because $E_1 \neq E_2$, $T_{oc}(z)$ depends on which value of E is chosen.

The transfer functions (15) and (18) have the same poles. The pronounced difference between them is the phase because the output voltages are sampled at different instants. For later reference, this new approach is called the SP method and the approach which uses the sampled output at $t = nT$ is called the S method.

2.6 Open-Loop Stability, Audio-Susceptibility, and Output Impedance

The matrix Φ_o determines the local open-loop orbital stability of the periodic solution $x^0(t)$. The next result follows from Eq. (12) (see [3] for a detailed prrof).

Theorem 2 *Assume that all of the eigenvalues of at least one of A_1 and A_2 are in the open left half of the complex plane, and that neither matrix has any eigenvalue in the open right half of*

the complex plane. Then the periodic solution $x^0(t)$ of the power stage of Fig. 2 is asymptotically orbitally stable.

The effects of disturbances at the source and load on the output voltage in the closed-loop system are related to open-loop audio-susceptibility and output impedance [8]. From Eqs. (10)-(11), the open-loop audio-susceptibility is

$$T_{os}(z) = \frac{\hat{v}_o(z)}{\hat{v}_s(z)} = E(zI - \Phi_o)^{-1}\Gamma_v \tag{19}$$

To calculate the open-loop output impedance, add a fictitious current source, i_o (as perturbation), in parallel with the load. Let

$$S_1 : \dot{x} = A_1 x + B_1 v_s + B_{i1} i_o \tag{20}$$

$$S_2 : \dot{x} = A_1 x + B_2 v_s + B_{i2} i_o \tag{21}$$

where $B_{i1}, B_{i2} \in \mathbf{R}^{N\times 1}$.

Similar to the open-loop audio-susceptibility, the open-loop output impedance is

$$T_{oo}(z) = \frac{\hat{v}_o(z)}{\hat{i}_o(z)} = E(zI - \Phi_o)^{-1}\Gamma_i \tag{22}$$

where

$$\Gamma_i = e^{A_2(T-d)} \int_0^d e^{A_1\sigma} d\sigma B_{i1} + \int_0^{T-d} e^{A_2\sigma} d\sigma B_{i2} \tag{23}$$

3 Discontinuous Conduction Mode (DCM) under Voltage Mode Control

The modeling and analysis steps taken in Sec. 2 are now applied to the DCM case. For brevity, the discussion of open-loop stability and the derivation of the open-loop audio-susceptibility and output impedance are omitted.

3.1 Block Diagram Model

A general model of the power stage of a PWM converter operating in DCM under voltage mode control is shown in Fig. 3. Similar to Eq. (18), the switching instant from S_1 to S_2 within the cycle is used as the control variable and denoted as d_{1n}. The matrix $F \in \mathbf{R}^{1\times N}$ is chosen such that $Fx = i_L$. The remaining notation is as in Fig. 2.

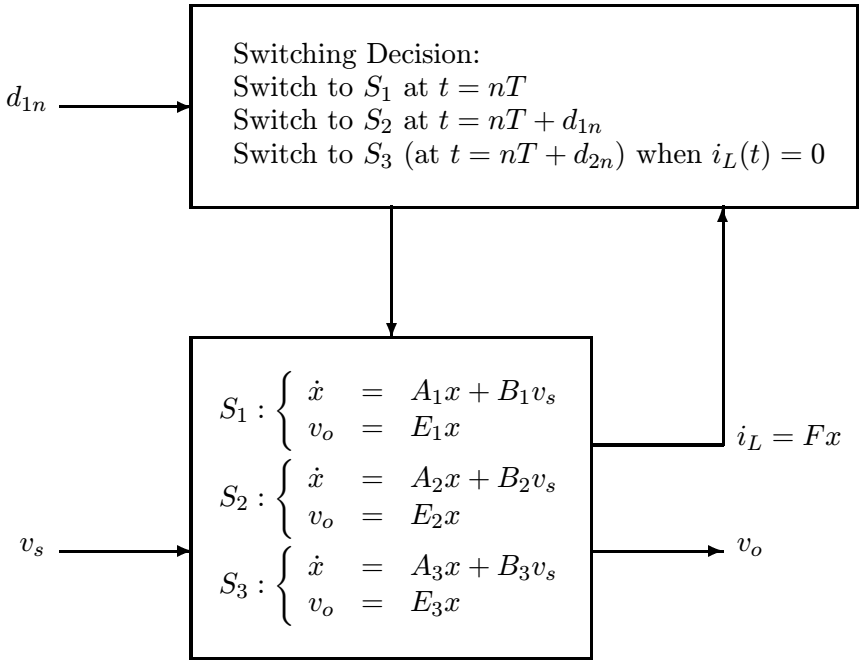

Figure 3: Power stage of PWM converter in DCM under voltage mode control

Compared with CCM, there is a third stage S_3 in DCM. Switching from S_1 to S_2 is controlled by the variable, d_{1n}. The system is switched from S_2 to S_3 when the inductor current $i_L = Fx$ reaches zero.

3.2 Nonlinear Sampled-Data Model

From the operation in Fig. 3, the sampled-data dynamics of the power stage is

$$\begin{aligned} x_{n+1} &= f(x_n, v_{sn}, d_{1n}, d_{2n}) \\ &= e^{A_3(T-d_{2n})}(e^{A_2(d_{2n}-d_{1n})}(e^{A_1d_{1n}}x_n + \int_0^{d_{1n}} e^{A_1(d_{1n}-\sigma)}d\sigma B_1 v_{sn}) \end{aligned}$$

$$+ \int_{d_{1n}}^{d_{2n}} e^{A_2(d_{2n}-\sigma)} d\sigma B_2 v_{sn}) + \int_{d_{2n}}^{T} e^{A_3(T-\sigma)} d\sigma B_3 v_{sn} \tag{24}$$

$$\hat{v}_{on} = E\hat{x}_n \tag{25}$$

$$\begin{aligned} g(x_n, v_{sn}, d_{1n}, d_{2n}) &= Fx(nT + d_{2n}) \\ &= F(e^{A_2(d_{2n}-d_{1n})}(e^{A_1 d_{1n}} x_n + \int_0^{d_{1n}} e^{A_1\sigma} d\sigma B_1 v_{sn}) \int_0^{d_{2n}-d_{1n}} e^{A_2\sigma} d\sigma B_2 v_{sn}) \\ &= 0 \end{aligned} \tag{26}$$

The variable d_{2n} is not a free variable but is constrained by Eq. (26). Another explicit constraint is $Fx_n = i_{Ln} = 0$, because the inductor current always starts from 0 at the beginning of a cycle. So the dynamics is $(N-1)$-dimensional instead of N-dimensional.

3.3 Calculation of Fixed Points (Periodic Solutions)

Let the nominal (set-point) output voltage at the clock time be $V_{\rm SET}$. The fixed point $(x_n, v_{sn}, d_{1n}, d_{2n}) = (x^0(0), V_s, d_1, d_2)$ of the sampled-data dynamics (24)-(26) should satisfy

$$x^0(0) = f(x^0(0), V_s, d_1, d_2) \tag{27}$$

$$V_{\rm SET} = Ex^0(0) \tag{28}$$

$$g(x^0(0), V_s, d_1, d_2) = 0 \tag{29}$$

Newton's method can be used to solve these $(N+2)$ equations in $(N+2)$ unknowns $(x^0(0), d_1, d_2)$.

3.4 Linearized Sampled-Data Dynamics

The system (24)-(26) can be linearized at the fixed point $(x^0(0), V_s, d_1, d_2)$. Using the notation $\diamond$ to denote evaluation at this fixed point,

$$\begin{aligned} \hat{x}_{n+1} &\approx \Phi_o \hat{x}_n + \Gamma_v \hat{v}_{sn} + \Gamma_d \hat{d}_{1n} \\ \hat{v}_{on} &= E\hat{x}_n \end{aligned} \tag{30}$$

where

$$\begin{aligned}
\Phi_o &= \frac{\partial f}{\partial x_n} - \frac{\partial f}{\partial d_{2n}}(\frac{\partial g}{\partial d_{2n}})^{-1}\frac{\partial g}{\partial x_n}\Big|_\diamond \\
&= e^{A_3(T-d_2)}(I - \frac{(\dot{x}^0(d_2^-) - \dot{x}^0(d_2^+))F}{F\dot{x}^0(d_2^-)})e^{A_2(d_2-d_1)}e^{A_1 d_1} \qquad (31)
\end{aligned}$$

$$\begin{aligned}
\Gamma_v &= \frac{\partial f}{\partial v_{sn}} - \frac{\partial f}{\partial d_{2n}}(\frac{\partial g}{\partial d_{2n}})^{-1}\frac{\partial g}{\partial v_{sn}}\Big|_\diamond \\
&= e^{A_3(T-d_2)}(e^{A_2(d_2-d_1)}\int_0^{d_1} e^{A_1\sigma}d\sigma B_1 + \int_0^{d_2-d_1} e^{A_2\sigma}d\sigma B_2) + \int_0^{T-d_2} e^{A_3\sigma}d\sigma B_3 \\
&\quad - \frac{\dot{x}^0(d_2^-) - \dot{x}^0(d_2^+)}{F\dot{x}^0(d_2^-)}F(e^{A_2(d_2-d_1)}\int_0^{d_1} e^{A_1\sigma}d\sigma B_1 + \int_0^{d_2-d_1} e^{A_2\sigma}d\sigma B_2) \qquad (32)
\end{aligned}$$

$$\begin{aligned}
\Gamma_d &= \frac{\partial f}{\partial d_{1n}} - \frac{\partial f}{\partial d_{2n}}(\frac{\partial g}{\partial d_{2n}})^{-1}\frac{\partial g}{\partial d_{1n}}\Big|_\diamond \\
&= e^{A_3(T-d_2)}(I - \frac{(\dot{x}^0(d_2^-) - \dot{x}^0(d_2^+))F}{F\dot{x}^0(d_2^-)})e^{A_2(d_2-d_1)}(\dot{x}^0(d_1^-) - \dot{x}^0(d_1^+)) \qquad (33)
\end{aligned}$$

The eigenvalues of Φ_o are the open-loop poles. Since the dynamics is $(N-1)$-dimensional, the determinant of Φ_o is expected to be 0. Indeed,

$$\det[\Phi_o] = \det[e^{A_2(d_2-d_1)}e^{A_1 d_1}e^{A_3(T-d_2)}](1 - \frac{F(\dot{x}^0(d_2^-) - \dot{x}^0(d_2^+))}{F\dot{x}^0(d_2^-)}) = 0$$

because $F\dot{x}^0(d_2^+) = \frac{d}{dt}i_L^0(d_2^+) = 0$.

3.5 Control-to-Output Transfer Function

As in CCM, the control-to-output transfer function in DCM is

$$T_{oc}(z) = \frac{\hat{v}_o(z)}{\hat{d}_1(z)} = Ee^{A_1 d_1}(zI - \Phi_o)^{-1}\Gamma_d + E\dot{x}^0(d_1^-) \qquad (34)$$

4 Continuous Conduction Mode under Current Mode Control

The idea of using the sampled-data method to model current mode control has been proposed in [9, 6]. Here this approach is illustrated more explicitly.

4.1 Block Diagram Model

In current mode control, the control variable is a command signal v_c which sets the peak inductor current in a cycle. When the switching frequency is high, v_c can be set constant in a cycle, denoted as v_{cn} in the $(n+1)$-st cycle. Denote by $h(t) = V_l + (V_h - V_l)\frac{t}{T} \bmod 1)$ the slope-compensating ramp. The switch is turned on when a clock pulse occurs, and turned off when the inductor current i_L reaches $v_{cn} - h(t)$. Denote by $nT + d_n$ the switching instant in the cycle when $i_L = v_{cn} - h(t)$.

A general model of the power stage of a PWM converter operated in CCM under current mode control is shown in Fig. 4, where the matrix $F \in \mathbf{R}^{1\times N}$ is chosen such that $Fx = i_L$. The remaining notation is the same as in Fig. 2.

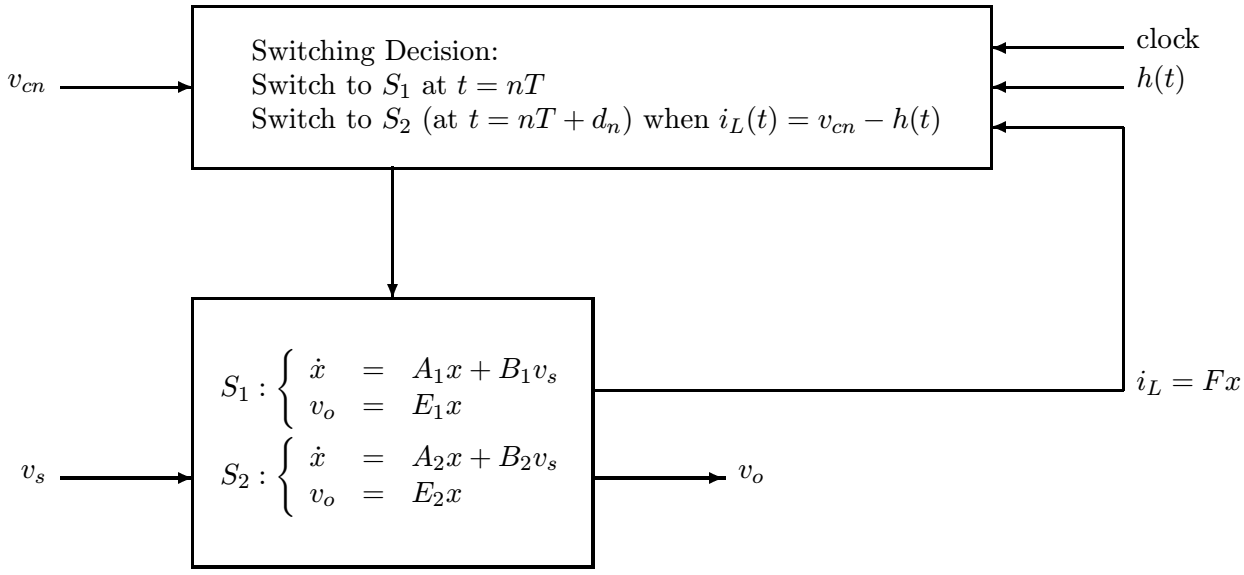

Figure 4: Power stage of PWM converter in CCM under current mode control

4.2 Nonlinear Sampled-Data Model

From Fig. 4 and the discussion above, the sampled-data dynamics of the power stage in CCM under current mode control is

$$\begin{array}{lcl} x_{n+1} & = & f(x_n, v_{sn}, d_n) \\ & = & e^{A_2(T-d_n)}(e^{A_1 d_n} x_n + \int_0^{d_n} e^{A_1\sigma} d\sigma B_1 v_{sn}) + \int_0^{T-d_n} e^{A_2\sigma} d\sigma B_2 v_{sn} \\ v_{on} & = & E x_n \\ g(x_n, v_{sn}, d_n, v_{cn}) & = & i_L(nT+d_n) - (v_{cn} - h(nT+d_n)) \\ & = & F(e^{A_1 d_n} x_n + \int_0^{d_n} e^{A_1\sigma} d\sigma B_1 v_{sn}) - v_{cn} + h(d_n) \\ & = & 0 \end{array} \tag{35}$$

4.3 Linearized Sampled-Data Dynamics

Assume there exists a fixed point $(x_n, v_{sn}, d_n, v_{cn}) = (x^0(0), V_s, d, V_c)$. Using the notation $\diamond$ to denote evaluation at this fixed point,

$$\hat{x}_{n+1} \approx \Phi_o \hat{x}_n + \Gamma_v \hat{v}_{sn} + \Gamma_c \hat{v}_{cn} \tag{36}$$

$$\hat{v}_{on} = E\hat{x}_n \tag{37}$$

where

$$\begin{array}{lcl} \Phi_o & = & \dfrac{\partial f}{\partial x_n} - \dfrac{\partial f}{\partial d_n}(\dfrac{\partial g}{\partial d_n})^{-1}\dfrac{\partial g}{\partial x_n}\Big|_\diamond \\ & = & e^{A_2(T-d)}(I - \dfrac{(\dot{x}^0(d^-) - \dot{x}^0(d^+))F}{F\dot{x}^0(d^-) + \dot{h}(d)})e^{A_1 d} \end{array} \tag{38}$$

$$\begin{array}{lcl} \Gamma_v & = & \dfrac{\partial f}{\partial v_{sn}} - \dfrac{\partial f}{\partial d_n}(\dfrac{\partial g}{\partial d_n})^{-1}\dfrac{\partial g}{\partial v_{sn}}\Big|_\diamond \\ & = & e^{A_2(T-d)}(I - \dfrac{(\dot{x}^0(d^-) - \dot{x}^0(d^+))F}{F\dot{x}^0(d^-) + \dot{h}(d)}) \displaystyle\int_0^d e^{A_1\sigma} d\sigma B_1 + \int_0^{T-d} e^{A_2\sigma} d\sigma B_2 \end{array} \tag{39}$$

$$\begin{array}{lcl} \Gamma_c & = & -\dfrac{\partial f}{\partial d_n}(\dfrac{\partial g}{\partial d_n})^{-1}\dfrac{\partial g}{\partial v_{cn}}\Big|_\diamond \\ & = & \dfrac{e^{A_2(T-d)}(\dot{x}^0(d^-) - \dot{x}^0(d^+))}{F\dot{x}^0(d^-) + \dot{h}(d)} \end{array} \tag{40}$$

The following result is similar to a stability result for closed-loop PWM converter in [1]. The proof is omitted.

Theorem 3 *If the periodic solution $x^0(t)$ is open-loop asymptotically orbitally stable, then the following inequality holds:*

$$\left|\frac{F\dot{x}^0(d^+)+\dot{h}(d)}{F\dot{x}^0(d^-)+\dot{h}(d)}\right| \leq e^{\mathrm{tr}[A_2-A_1]d-\mathrm{tr}[A_2]T} \tag{41}$$

Remark: Generally the switching period is so small that the right side of (41) can be approximated as 1, resulting in a condition that resembles a well-known stability criterion in current mode control [8, for example]:

$$\left|\frac{m_2-m_c}{m_1-m_c}\right| < 1 \tag{42}$$

where m_1 and -m_2 are the slopes of current trajectories during the on and off stages respectively using a *linear approximation* [10], and m_c is the slope of the compensating ramp. The stability criterion (42) differs from Theorem 3, in which the *instantaneous* slope is used. Also, Theorem 3 applies to the *open-loop* system.

4.4 Control-to-Output Transfer Function

From the discussion in Sec. 2.5, it is reasonable to use the output sampled at $t = nT + d_n$ rather than at $t = nT$ for the control-to-output transfer function.

The output equation in this case is

$$\begin{aligned} v_{on} &= Ex(nT+d_n) \\ &= E(e^{A_1 d_n}x_n + \int_0^{d_n} e^{A_1\sigma}d\sigma B_1 v_{sn}) := l(x_n, v_{sn}, d_n) \end{aligned} \tag{43}$$

with linearized dynamics

$$\hat{v}_{on} \approx \Lambda_x\hat{x}_n + \Lambda_c\hat{v}_{cn} + \Lambda_v\hat{v}_{sn} \tag{44}$$

where

$$\Lambda_x = \frac{\partial l}{\partial x_n} - \frac{\partial l}{\partial d_n}(\frac{\partial g}{\partial d_n})^{-1}\frac{\partial g}{\partial x_n}\Big|_\diamond = E(I - \frac{\dot{x}^0(d^-)F}{F\dot{x}^0(d^-) + \dot{h}(d)})e^{A_1 d} \tag{45}$$

$$\Lambda_c = -\frac{\partial l}{\partial d_n}(\frac{\partial g}{\partial d_n})^{-1}\frac{\partial g}{\partial v_{cn}}\Big|_\diamond = \frac{E\dot{x}^0(d^-)}{F\dot{x}^0(d^-) + \dot{h}(d)} \tag{46}$$

$$\Lambda_v = \frac{\partial l}{\partial v_{sn}} - \frac{\partial l}{\partial d_n}(\frac{\partial g}{\partial d_n})^{-1}\frac{\partial g}{\partial v_{sn}}\Big|_\diamond = E(I - \frac{\dot{x}^0(d^-)F}{F\dot{x}^0(d^-) + \dot{h}(d)})\int_0^d e^{A_1\sigma}d\sigma B_1 \tag{47}$$

From the linearized dynamics (36) and (44), the control-to-output transfer function is

$$T_{oc}(z) = \frac{\hat{v}_o(z)}{\hat{v}_c(z)} = \Lambda_x(zI - \Phi_o)^{-1}\Gamma_c + \Lambda_c \tag{48}$$

5 Continuous-Time Power Stage Model Obtained from Sampled-Data Model

Two sampled-data dynamic models of the power stage have been derived, using the S and SP methods. The sampled-data dynamics using the S method is useful for discrete-time controller design. The sampled-data dynamics using the SP method has better control-to-output frequency response, which is useful for analog controller design. Frequency response information suffices for the practical controller design. In some cases, continuous-time dynamical equations of the power stage are needed. For instance, such a model facilitates analog feedback control design for PWM converters. In this section, a continuous-time model of the power stage will be derived for which the control-to-output frequency response is close to that of the sampled-data model. This continuous-time model differs from the traditional averaged model, which is independent of the switching frequency.

In obtaining the approximate continuous-time model from the sampled-data linearized model, it should be recognized that some of the benefits of sampled-data modeling are compromised. Most importantly, the duty cycle, which is best viewed as a function that changes in discrete steps from

cycle to cycle, is viewed as a smooth function in continuous-time. The averaging method also uses such an approximate description of the duty cycle.

Given a linear sampled-data model, there are many ways to derive a continuous-time model with a similar frequency response [11]. Here one approach is proposed. Without loss of generality, such a continuous-time model will be obtained for the circuit operation in CCM under voltage mode control. The linearized sampled-data dynamics of the power stage using SP method is (10) with (17). Transforming ("lifting") the sampled-data pair $(\Phi_o, [\Gamma_v, \Gamma_d])$ to the continuous-time pair $(\Phi_o^c, [\Gamma_v^c, \Gamma_d^c])$ by the technique in Appendix A, the following continuous-time model of the power stage is proposed:

$$\begin{array}{rcl} \dot{\hat{x}} & = & \Phi_o^c \hat{x} + \Gamma_v^c \hat{v_s} + \Gamma_d^c \hat{d} \\ \hat{v}_o & = & E e^{A_1 d} \hat{x} + E \dot{x}^0(d^-) \hat{d} \end{array} \tag{49}$$

The control-to-output transfer function in the lifted dynamics (49) is

$$T_{oc}^c(s) = E e^{A_1 d}(sI - \Phi_o^c)^{-1} \Gamma_d^c + E \dot{x}^0(d^-) \tag{50}$$

6 Illustrative Examples

As mentioned in the Introduction, the main motivation for careful modeling of the power stage is to facilitate controller design. To verify the validity of power stage models, a feedback loop is set up. Generally the controller for PWM converter uses dynamic feedback, with an integrator enclosed. For simplicity, static feedback is used. Accuracy of the sampled-data models will be illustrated by examples taken from the literature.

Example 1 (*Buck converter in CCM under voltage mode control with leading edge modulation*, [12]) Consider the buck converter under voltage mode control shown in Fig. 5. Let $T = 400\mu s$, $L = 20mH$, $C = 47\mu F$, $R = 22\Omega$, $V_r = 11.3V$, $g_1 = 8.4$, $V_l = 3.8V$, $V_h = 8.2V$, and $h(t) = V_l + (V_h - V_l)[\frac{t}{T} \bmod 1]$. The system has been shown to be unstable for $V_s > 24.527$ in [12] by computer simulation and in [13, 3] by closed-loop analysis.

However the system is predicted to be stable for $15 < V_s < 40$ if the averaging method is used [14].

Next the sampled-data method is used. The state matrices in Fig. 2 are

$$\begin{aligned} A_1 &= A_2 = \begin{bmatrix} 0 & \frac{-1}{L} \\ \frac{1}{C} & \frac{-1}{RC} \end{bmatrix} \\ B_1 &= \begin{bmatrix} 0 \\ 0 \end{bmatrix} \qquad\qquad B_2 = \begin{bmatrix} \frac{1}{L} \\ 0 \end{bmatrix} \\ E_1 &= E_2 = \begin{bmatrix} 0 & 1 \end{bmatrix} \end{aligned}$$

Take $V_s = 20$ for example. The duty cycle D_c can be estimated from the switching condition

$$g_1(V_s D_c - V_r) = (1 - D)(V_h - V_l) + V_l$$

This gives $D_c = 0.598$. Then $d = (1 - D_c)T = 1.6074 \times 10^{-6}$. From Eq. (18), the duty-ratio-to-output transfer function is $(-T)T_{oc}(z)$, where the negative sign is because of leading edge modulation. The corresponding frequency response is shown in Fig. 6. The gain margin is 7.2 dB. The error amplifier and PWM modulator contribute a gain $g_1/(V_h - V_l) = 5.6165$ dB. Thus the gain which V_s can increase by [1] without causing instability is $7.2 - 5.6165 = 1.5835$ dB (1.20). This means that the system will be unstable for $V_s > 20 \times 1.20 = 24.0$. The prediction of closed-loop instability is very good.

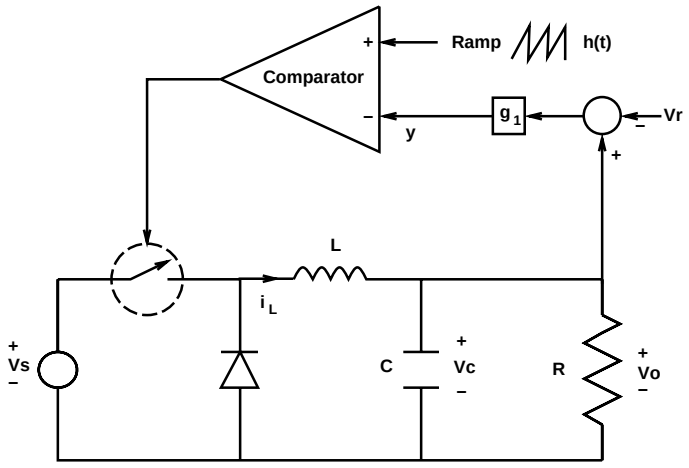

Figure 5: System diagram for Example 1

Example 2 (Boost converter in DCM under voltage mode control, [15]) The power stage of a boost converter is shown in Fig. 7, where the system parameters are $f_s = 3kHz$, $V_s = 16V$,

[1] It can be seen from Eqs. (5) and (18) that V_s contributes linearly to the open-loop gain.

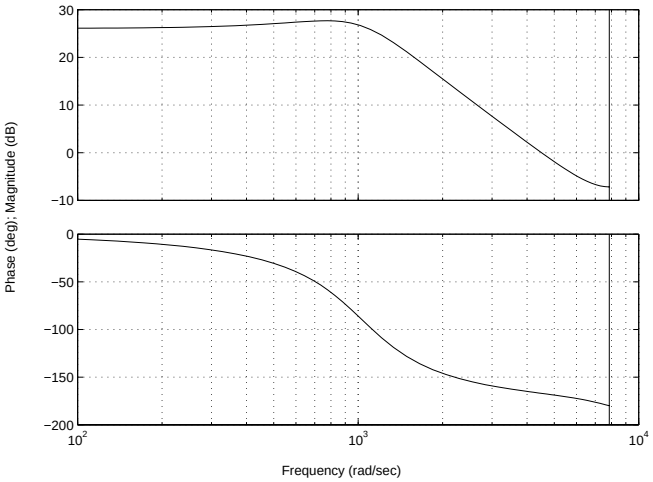

Figure 6: Duty-ratio-to-output frequency response for Example 1

$R = 12.5\Omega$, $L = 208\mu H$, $C = 222\mu F$, $R_c = 0$ and $V_{\rm SET} = 25V$. The converter has been shown to be unstable for the feedback gain greater than 0.08 by simulation [15].

The state matrices in Fig. 3 are

$$\begin{array}{rclcrcl} A_1 & = & A_3 = \left[\begin{array}{cc} 0 & 0 \\ 0 & \frac{-1}{RC} \end{array}\right] & & A_2 & = & \left[\begin{array}{cc} 0 & \frac{-1}{L} \\ \frac{1}{C} & \frac{-1}{RC} \end{array}\right] \\ B_1 & = & B_2 = \left[\begin{array}{c} \frac{1}{L} \\ 0 \end{array}\right] & & B_3 & = & \left[\begin{array}{c} 0 \\ 0 \end{array}\right] \\ E_1 & = & E_2 = E_3 = \left[\begin{array}{cc} 0 & 1 \end{array}\right] & & F & = & \left[\begin{array}{cc} 1 & 0 \end{array}\right] \end{array} \tag{51}$$

Solving Eqs. (27)-(29) by Newton's method gives $d_1 = 0.0001$ (hence $D_c = 0.3$) and $d_2 = 0.00027$.

From Eq. (34), the duty-ratio-to-output transfer function is $T_{oc}(z)T$. The corresponding frequency response is shown in Fig. 8. The gain margin is -22.66 dB (0.0736). So a feedback gain greater than 0.0736 is predicted to be destabilizing, which is close to the result of [15] noted above.

Example 3 (*Boost converter in DCM under voltage mode control*, [8, p.389]) The power stage of a boost converter is shown in Fig. 7, where the system parameters are $f_s = 100kHz$, $V_s = 24V$, $R = 12\Omega$, $L = 5\mu H$, $C = 470\mu F$, $R_c = 0$ and $V_{\rm SET} = 36V$.

In [8], two averaged models are used to study this circuit. One model is 1-dimensional, and

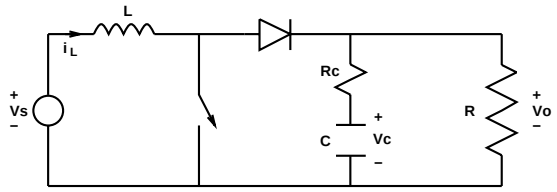

Figure 7: Boost converter with source voltage and resistive load

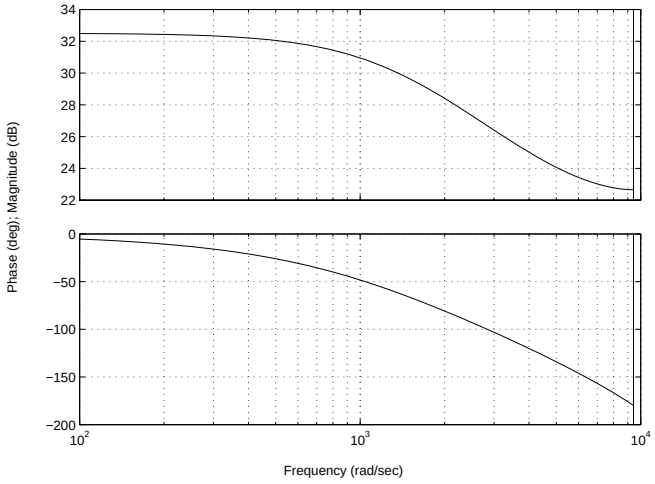

Figure 8: Duty-ratio-to-output frequency response for Example 2

its duty-ratio-to-output frequency response has infinite gain margin. The second model (based on [16]) has gain margin of 33 dB.

Next, consider the sampled-data model of this circuit. The state matrices in Fig. 3 are the same as in Eq. (51). Solving Eqs. (27)-(29) by Newton's method gives $d_1 = 2.5 \times 10^{-6}$ (hence $D_c = 0.25$), $d_2 = 7.4978 \times 10^{-6}$ and $x^0(d_1) = (i_L^0(d_1), v_C^0(d_1)) = (12, 35.98)$. From Eq. (34), the duty-ratio-to-output transfer function is $T_{oc}(z)T$. The corresponding frequency response is shown in Fig. 9, from which the gain margin is found to be 9.91 dB.

To ascertain which of these models gives the best result, a feedback loop (Fig. 10) is added to the power stage. As the gain g varies, the nominal periodic solution $x^0(t)$ also varies. To keep the nominal periodic solution the same, the reference voltage is varied according to $V_r = \frac{h(d_1)}{g} + v_C^0(d_1) = \frac{0.25}{g} + 35.98$. Using the exact closed-loop analysis in [1], the system is found to become unstable for gains $g > 3.13$ (9.91 dB). Thus the sampled-data model has given accurate prediction of the gain margin.

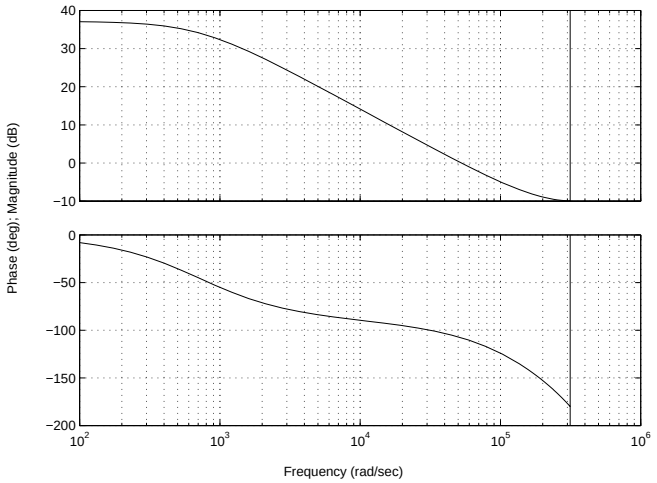

Figure 9: Duty-ratio-to-output frequency response for Example 3

Example 4 (*Boost converter in CCM under current mode control*, [17]) The power stage of a boost converter is shown in Fig. 7, where the system parameters are $f_s = 100kHz$, $V_s = 5V$, $R = 15\Omega$, $L = 40\mu H$, $C = 200\mu F$, $R_c = 0$ and $D_c = 0.5951$.

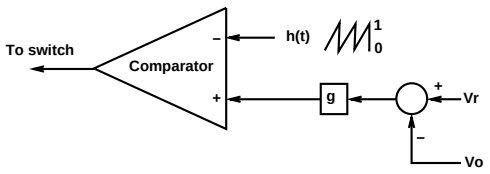

Figure 10: Simple static feedback for PWM converter under voltage mode control

In [17], three averaged models are compared. The duty-ratio-to-output frequency response for each one has gain margin 29.7 dB, 29.7 dB and 29.6 dB, respectively.

Next the sampled-data model is applied. The matrices in Fig. 4 are the same as in Eq. (51). Calculating the fixed point in Eq. (35) gives $x^0(0) = (1.661, 12.3599)$ and $x^0(d) = (2.4049, 12.3354)$. From Eq. (48), the duty-ratio-to-output transfer function is $T_{oc}(z)T$. The corresponding frequency response is shown in Fig. 11. The gain margin is 28.035 dB (25.2525).

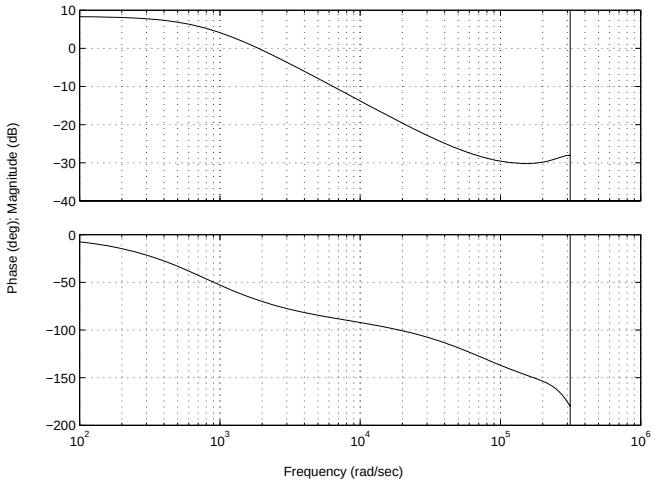

Figure 11: Duty-ratio-to-output frequency response for Example 4

A feedback loop (Fig. 12) is set up. As the gain g varies, the nominal periodic solution $x^0(t)$ also varies. To keep the nominal periodic solution the same, the reference voltage is varied according to $V_r = \frac{h(d)+i_L^0(d)}{g} + v_C^0(d) = \frac{3}{g} + 12.3354$. Using the exact closed-loop analysis in [1], the system is unstable for gains $g > 25.6803$ (28.192 dB). When $g = 25.6803$, the closed-loop eigenvalues are $0.3203 \pm 0.9474i$ (on the unit circle). Thus a Neimark-Sacker bifurcation [3] occurs. It is surprising

to see such a bifurcation occurring in a converter under current mode control.

From this example, the sampled-data model of the power stage predicts closed-loop instability more accurately than any of the three averaged models in [17].

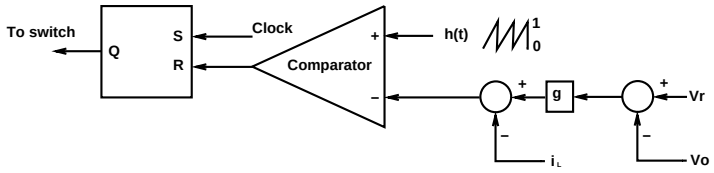

Figure 12: Simple static feedback for PWM converter under current mode control

7 Concluding Remarks

Sampled-data models and associated analysis have been developed for the power stage of the PWM converter. Several configurations have been considered, including DCM or CCM under voltage mode control, and CCM under current mode control. Compared with the derivations of averaged models in DCM or under current mode control, the sampled-data approach is more systematic. A new continuous-time linear model of the power stage was also obtained by employing a simple transformation on the sampled-data model. Control design using the newly developed power stage models was illustrated using several examples from the literature. The predictions were tested against the exact closed-loop model of the companion paper [1]. The predictions based on the power stage models were found to be highly accurate. It is hoped that the new models will facilitate improved controller designs for PWM DC-DC converters.

Acknowledgments

This research has been supported in part by the the Office of Naval Research under Multidisciplinary University Research Initiative (MURI) Grant N00014-96-1-1123, the U.S. Air Force Office of Scientific Research under Grant F49620-96-1-0161, and by a Senior Fulbright Scholar Award.

References

[1] C.-C. Fang and E.H. Abed, "Sampled-data modeling and analysis of PWM DC-DC converters I. Closed-loop circuits," preprint, Feb. 1998.

[2] F.C.Y. Lee, R.P. Iwens, Yuan Yu, and J.E. Triner, "Generalized computer-aided discrete time-domain modeling and analysis of DC-DC converters," *IEEE Transactions on Industrial Electronics and Control Instrumentation*, vol. IECI-26, no. 2, pp. 58–69, 1979.

[3] C.-C. Fang, *Sampled-Data Analysis and Control of DC-DC Switching Converters*, Ph.D. thesis, University of Maryland, College Park, 1997.

[4] F. Garofalo, P. Marino, S. Scala, and F. Vasca, "Control of DC-DC converters with linear optimal feedback and nonlinear feedforward," *IEEE Transactions on Power Electronics*, vol. 9, no. 6, pp. 607–615, 1994.

[5] C.-C. Fang and E.H. Abed, "Discrete-time integral control of PWM DC-DC converters," preprint, Sept. 1998.

[6] J.G. Kassakian, M.F. Schlecht, and G.C. Verghese, *Principles of Power Electronics*, Addison-Wesley, Reading, MA, 1991.

[7] A.V. Oppenheim and R.W. Schafer, *Discrete-Time Signal Processing*, Prentice-Hall, Englewood Cliffs, NJ, 1989.

[8] R.W. Erickson, *Fundamentals of Power Electronics*, Chapman and Hall, New York, 1997.

[9] G.C. Verghese, C.A. Bruzos, and K.N. Mahabir, "Averaged and sampled-data models for current mode control: a re-examination," in *IEEE Power Electronics Specialists Conf. Rec.*, 1989, pp. 484–491.

[10] R.D. Middlebrook and S. Ćuk, "A general unified approach to modelling switching-converter power stages," in *IEEE Power Electronics Specialists Conf. Rec.*, 1976, pp. 18–34.

[11] G.F. Franklin, D. Powell, and M.L. Workman, *Digital Control of Dynamic Systems*, Addison-Wesley, Reading, Mass., Second edition, 1990.

[12] D.C. Hamill, J.H.B. Deane, and J. Jefferies, "Modeling of chaotic DC-DC converters by iterated nonlinear mappings," *IEEE Transactions on Power Electronics*, vol. 7, no. 1, pp. 25–36, 1992.

[13] E. Fossas and G. Olivar, "Study of chaos in the buck converter," *IEEE Transactions on Circuits and Systems-I: Fundamental Theory and Applications*, vol. 43, no. 1, pp. 13–25, 1996.

[14] D.C. Hamill, "Power electronics: A field rich in nonlinear dynamics," in *Nonlinear Dynamics of Electronic Systems*, Dublin, 1995.

[15] C.K. Tse, "Flip bifurcation and chaos in three-state boost switching regulators," *IEEE Transactions on Circuits and Systems-I: Fundamental Theory and Applications*, vol. 41, no. 1, pp. 16–23, 1994.

[16] V. Vorperian, "Simplified analysis of PWM converters using model of PWM switch. II. Discontinuous conduction mode," *IEEE Transactions on Aerospace and Electronic Systems*, vol. 26, no. 3, pp. 497–505, 1990.

[17] J. Sun and R. Bass, "A new approach to averaged modeling of PWM converters with current-mode control," in *Proceedings of International Conference on Industrial Electronics, Control, and Instrumentation*, 1997.

Appendix A Discretizing a Continuous-Time System Through a Zero-Order-Hold

Consider a linear continuous-time system

$$\begin{aligned} \dot{x} &= Ax + Bu \\ y &= Ex \end{aligned} \tag{52}$$

where $A \in \mathbf{R}^{N\times N}$, $B \in \mathbf{R}^{N\times 1}$, $E \in \mathbf{R}^{1\times N}$, $x \in \mathbf{R}^N$, and $y, u \in \mathbf{R}$.

To obtain a discrete-time model from this continuous-time system, a zero-order-hold is inserted before the input signal, and the output is sampled using a sampling interval T equal to the duration of the zero-order-hold; see Fig. 13. This involves an assumption that the input varies slowly enough to be considered constant within intervals of length T.

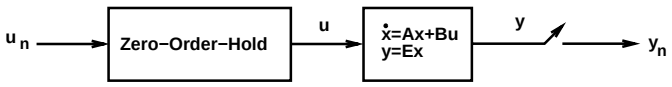

Figure 13: Discretizing a continuous-time system through a zero-order-hold

The discrete-time system has the dynamics

$$\begin{aligned} x_{n+1} &= \Phi x_n + \Gamma u_n \\ y_n &= Ex_n \end{aligned} \tag{53}$$

where

$$\Phi = e^{AT} \tag{54}$$

$$\Gamma = \int_0^T e^{A\sigma} d\sigma B \tag{55}$$

The following fact facilitates converting back to the the continuous-time pair (A, B) from knowledge of the discrete-time pair (Φ, Γ) and T. This process of converting back may be thought of as "lifting" the discrete-time dynamics to obtain a consistent continuous-time system.

Fact 1

$$\begin{bmatrix} \Phi & \Gamma \\ 0 & 1 \end{bmatrix} = \exp\left(\begin{bmatrix} A & B \\ 0 & 0 \end{bmatrix} T\right)$$

The input-to-output transfer function in the continuous-time domain is

$$E(sI - A)^{-1}B \tag{56}$$

The input-to-output transfer function in the discrete-time domain is

$$E(zI - \Phi)^{-1}\Gamma \tag{57}$$

Given the discrete-time dynamics (53) and the value of T, the continuous-time transfer function (56) can be obtained by using Fact 1.